Inorganic Chemistry

Article

pubs.acs.org/IC

Cationic Clathrate of Type-III $Ge_{172-x}P_xTe_y$ ($y \approx 21.5$, $x \approx 2y$): Synthesis, Crystal Structure and Thermoelectric Properties

Maria A. Kirsanova,[†] Takao Mori,[‡] Satofumi Maruyama,[‡] Artem M. Abakumov,[§] Gustaaf Van Tendeloo,[§] Andrei Olenev,[∥] and Andrei V. Shevelkov*,[†]

[†]Department of Chemistry, Lomonosov Moscow State University, Leninskie Gory 1-3, Moscow 119991, Russia

[‡]International Center for Materials Nanoarchitectonics (MANA), National Institute for Materials Science (NIMS), 305-0044 Tsukuba, Japan

[§]EMAT, University of Antwerp, Groenenborgerlaan 171, B-2020, Antwerp, Belgium

[∥]"SineTheta" Ltd., scientific park of Lomonosov Moscow State University, Leninskie Gory, 1-77, Moscow 119991, Russia

Supporting Information

ABSTRACT: A first germanium-based cationic clathrate of type-III, $Ge_{129.3}P_{42.7}Te_{21.53}$, was synthesized and structurally characterized (space group $P4_2/mnm$, a = 19.948(3) Å, c = 10.440(2) Å, Z = 1). In its crystal structure, germanium and phosphorus atoms form three types of polyhedral cages centered with Te atoms. The polyhedra share pentagonal and hexagonal faces to form a 3D framework. Despite the complexity of the crystal structure, the $Ge_{129.3}P_{42.7}Te_{21.53}$ composition corresponds to the Zintl counting scheme with a good accuracy. $Ge_{129.3}P_{42.7}Te_{21.53}$ demonstrates semiconducting/insulating behavior of electric resistivity, high positive Seebeck coefficient (500 μV K^{-1} at 300 K), and low thermal conductivity (<0.92 W m^{-1} K^{-1}) within the measured temperature range.

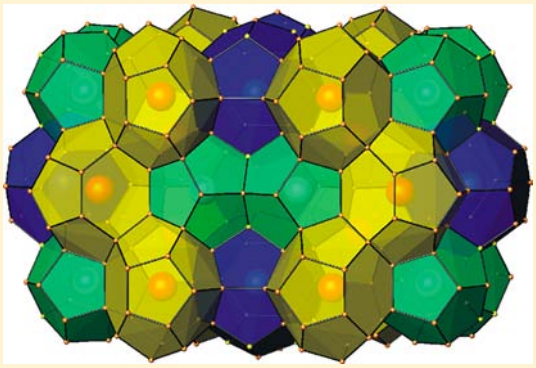

INTRODUCTION

The term "clathrates" refers to several well-known structure types, which can be represented as a specific three-dimensional network with large cavities filled with guest atoms or molecules. The latter do not form strong covalent bonds with the framework and are kept within the cavities by weak electrostatic interactions. Gas hydrates were the first representatives of the clathrate family.[1,2] Their framework is built up from water molecules, whereas the gas molecules, such as Cl_2 or SO_2, serve as guests. In the middle of the 1960s Kasper et al. revealed that sodium silicides Na_8Si_{46} and Na_xSi_{136} adopted the same crystal structure as various gas hydrates.[3] Afterward, a large group of inorganic clathrates based on the group 14 elements was discovered. They have been intensively investigated because of their prospective thermoelectric properties. Some of them, for instance, $Ba_8Ge_{30}Ga_{16}$ and $Ba_8Au_{5.3}Ge_{40.7}$, show high values of the thermoelectric figure of merit ZT at relatively high temperature.[4]

Several types of the clathrate crystal structures are documented in the literature.[2,5] They are usually noted as clathrate-I, clathrate-II, and so forth. Each structural type is characterized by a definite shape of guest-filled polyhedra and a manner of their packing. The overwhelming majority of inorganic clathrates crystallize in the type-I structure, whereas other structure types consist of only a limited number of representatives. In particular, only few type-III clathrates are known, starting from the discovery of the bromine hydrate $[H_2O]_{172}(Br_2)_{20}\square_{10}$.[6] Later, this family was expanded by the compounds of the group 14 elements.[7−9] Two of them have frameworks built up mainly of tin atoms and incorporate alkali metal atoms as cationic guests. Another compound is $Si_{130}P_{42}Te_{21}$, which features silicon as the main framework-forming element and tellurium as the anionic guest, demonstrating a reversal of the host−guest polarity.[10] Although clathrates of type-III have not been known for germanium, clathrates with an inversed polarity are not rare for this element. Cationic clathrates $[Ge_{38}Pn_8]X_8$ (Pn = P, As, Sb; X = Cl, Br, I), which crystallize in the clathrate-I type structure, were reported by Menke and von Schnering.[11] Recently $Ge_{79}P_{29}S_{18}Te_6$ with a new type of clathrate structure (clathrate-X) was discovered.[12]

Clathrates are also an interesting class of compounds studied for possible thermoelectric applications.[4,5,13] In general, their melting points are not so high compared to other classes of investigated thermoelectric materials, such as skutterudites,[14] germanium silicides,[15] boron carbide[16] and boron cluster-based compounds,[17] oxides,[18] and $Yb_{14}MnSb_{11}$.[19] However, previously clathrates in the Si−P−Te system were found to exhibit the highest known melting points among clathrates along with good high temperature thermoelectric properties.[9] With this in mind we have further investigated related cationic clathrate compounds.

Received: May 14, 2013
Published: June 26, 2013

   dx.doi.org/10.1021/ic401203r | Inorg. Chem. 2013, 52, 8272−8279

In this work we report on the synthesis, crystal structure, and thermoelectric properties of a first germanium-based cationic type-III clathrate $Ge_{129.3}P_{42.7}Te_{21.53}$.

EXPERIMENTAL SECTION

1. Synthesis and Characterization by X-ray Powder Diffraction (XRPD). The following starting materials were used for the synthesis: red P powder (98%), Ge powder (100 mesh, 99.999%), Te pieces (99.99%). Red phosphorus was purified by a standard method.[20] GeP was first synthesized and used as a precursor. To prepare GeP, the elemental substances were mixed in stoichiometric amounts with the total weight of 0.5 g, sealed in a silica ampule under vacuum, and annealed at 875 K for 5 days. The synthesis of $Ge_{129.3}P_{42.7}Te_{21.53}$ was performed starting from the stoichiometric mixture of GeP, Ge, and Te. They were placed in sealed silica tubes and annealed in vertical furnaces at a temperature of 953 K for 72 h. After the first annealing the sample always contained a ∼10−15 wt % admixture of germanium and a small amount of phosphorus in the upper tip of the ampule. To reach the equilibrium state, further annealings were carried out at 873 K for 120 h with the addition of a constant amount of phosphorus, creating a partial pressure of ∼1 bar inside the ampule.

The obtained samples were investigated by X-ray powder diffraction (XRPD) using a STOE STADI-P diffractometer (Cu−$K_{\alpha 1}$ radiation, transmission mode) and a Huber G670 image plate Guinier camera (Cu−$K_{\alpha 1}$ radiation, transmission mode) at room temperature. The unit cell parameters were calculated and refined from least-squares fits using Ge (a = 5.6576 Å) as an internal standard.

2. Single-Crystal X-ray Diffraction. From the sample obtained at 875 K a small crystal was selected for a single crystal X-ray diffraction experiment. Diffraction data were collected on a CAD-4 (NONIUS) diffractometer (Mo−K_α) at room temperature. For the refinement of the unit cell parameters a basis of 24 reflections in the range of 15.8° < θ < 17.1° was selected. The data were corrected by a semiempirical absorption correction based on azimutal scans of several reflections with χ angles close to 90°.

The collected data were processed using the SHELX-97 package.[21] The crystal structure was solved by direct methods and refined by full-matrix least-squares fits against F^2 in an anisotropic approximation, resulting in the composition $Ge_{129.3(3)}P_{42.7(3)}Te_{21.53(3)}$. Detailed crystallographic information is collected in Tables 1 and 2. Further details on the crystal structure investigation may be obtained from the Fachinformationszentrum Karlsruhe, D-76344 Eggenstein-Leopoldshafen, Germany (fax: +(49)7247−808−666; e-mail: crysdata@fiz-karlsruhe.de) by quoting the number CSD- 425439.

3. Energy-Dispersive X-ray (EDX) Analysis. EDX analysis was carried out on a powder sample by means of a JEOL JSM-5510 scanning electron microscope operating at 20 kV and equipped with an Oxford Instruments detector system. The data were collected from several regions selected on different crystals, the results were averaged and normalized to a total of 172 Ge and P atoms, leading to the gross formulas $Ge_{127(2)}P_{45(2)}Te_{19(2)}$.

4. Transmission Electron Microscopy. Samples for transmission electron microscopy (TEM) were prepared by grinding the sample in ethanol and depositing drops of suspension onto holey carbon grids. Selected area electron diffraction (SAED) was performed on a Philips CM20 electron microscope; high angle annular dark field scanning transmission electron microscopy (HAADF-STEM) observations were performed with a FEI Tecnai G2 electron microscope operated at 200 kV. The simulation of images from the structure data was done using the QSTEM software.[22]

5. Thermal Analysis. Differential scanning calorimetry (DSC) and thermogravimetric (TG) measurements were carried out with an STA409 TG/DSC analyzer (Netzsch). About 17 mg of the material was placed in a corundum crucible and heated up to 1273 K in a dry argon flow at a heating rate of 10 K min^{-1}.

6. Physical Property Measurements. The powder of the clathrate phase was compacted by spark plasma sintering (SPS) at a pressure of 60 MPa and a temperature of 773 K in an argon atmosphere with the use of a LABOX-625 (SINTER LAND) apparatus. A rectangular shaped sample (1.6 mm × 7.0 mm × 7.0 mm) with the density of 4.95 g cm^{-3} (92−93% of the theoretical density) was cut from the SPS-prepared product and used for the measurements. The rest of the sample was used for the XRPD analysis, which revealed less than 5 wt % admixture of Ge.

The electrical resistivity and thermoelectric power were measured with an ULVAC ZEM-2 apparatus in a helium atmosphere by using the four probe method and differential method, respectively. The temperature range of the measurements was from 300 to 660 K. To determine the thermal conductivity, first of all, the room temperature specific heat was measured by using a transient heat pulse method with a small temperature increase of 2% relative to the system temperature. Then, the relative specific heat and thermal diffusivity coefficient were measured by a laser flash method from 300 to 660 K with an ULVAC TC-7000 machine. The thermal conductivity is determined as the product of the density, specific heat, and thermal diffusivity coefficient.

Table 1. Data Collection and Structure Refinement Parameters for $Ge_{129.3}P_{42.7}Te_{21.53}$

composition	$Ge_{129.3(3)}P_{42.7(3)}Te_{21.53(3)}$
space group	$P4_2/mnm$ (No. 136)
M_r [g mol^{-1}]	13454.70
cell parameters [Å]	$a = b$ = 19.948(3)
	c = 10.440(2)
V [Å^3]	4154.3(12)
T [K]	293(2)
Z	1
radiation, λ [Å]	MoK_α, 0.71073
ρ_{calc}, [g·cm^{-3}]	5.378
μ [mm^{-1}]	27.098
θ range [deg]	2.04 < θ < 29.97
reflections collected/unique	6387/3294 [R(int) = 0.0780]
data/parameter	3294/146
R_1, wR_2 [$I > 2\sigma(I)$]	0.0543, 0.1401
goodness-of-fit on F^2	1.059

RESULTS AND DISCUSSION

1. Synthesis and Composition. The synthesis of pure $Ge_{129.3}P_{42.7}Te_{21.53}$ can be performed starting from the stoichiometric mixture of GeP, Ge, and Te according to the procedure described in the Experimental Section. The parameters of the tetragonal unit cell of the clathrate phase were calculated after each stage of the synthesis and appeared to be equal within the accuracy of determination. The XRPD pattern of the pure clathrate sample was refined by the Rietveld method (Figure 1) using the single crystal structure data (see below). According to the EDX analysis, the composition of the sample is $Ge_{127(2)}P_{45(2)}Te_{19(2)}$ which is in good agreement with the composition derived from the crystal structure refinement. The sample prepared at the given conditions was further used for the investigation by TEM and measurements of physical properties.

In attempts to improve the synthesis of the clathrate phase, the (possible) homogeneity range of the $Ge_{172-x}P_xTe_y$ solid solutions has been investigated for x varying from 30 to 60 and y varying from 10 to 30. The obtained samples contained small amounts of Ge and GeTe as admixtures because of partial P evaporation into the ampule volume. A combination of the EDX and XRD analyses showed a variation of the lattice parameters concomitant with the chemical composition. The unit cell parameters vary from a = 19.958(2) Å and c = 10.453(7) Å to a = 20.110(6) Å and c = 10.4780(4) Å, indicating the existence of a homogeneity range, whose exact

dx.doi.org/10.1021/ic401203r | Inorg. Chem. 2013, 52, 8272−8279

Table 2. Atomic Coordinates, Site Occupancies, and Equivalent Isotropic Displacement Parameters for $Ge_{129.3}P_{42.7}Te_{21.53}$

atom	Wyckoff	*x/a*	*y/b*	*z/c*	s.o.f.	U_{iso}, Å^2
Te(1)	4*g*	0.5991(1)	0.4009(1)	0	1	0.027(1)
Te(2)	8*j*	0.3186(1)	0.3186(1)	0.2513(1)	1	0.017(1)
Te(3)	8*i*	0.4668(1)	0.8705(1)	0	1	0.017(1)
Te(4)	8*i*	0.5657(3)	0.2452(3)	0.5000	0.193(4)	0.012(2)
P(1)	8*j*	0.1853(1)	0.1853(1)	0.1848(3)	1	0.007(1)
P(2)	16*k*	0.4985(1)	0.3661(1)	0.6853(2)	1	0.009(1)
Ge(1)	4*f*	0.2359(1)	0.2359(1)	0	1	0.014(1)
Ge(2)	4*d*	0.5000	0	0.7500	1	0.011(1)
Ge(3)	4*f*	0.4051(1)	0.4051(1)	0	1	0.018(1)
Ge(4)	8*i*	0.6941(1)	0.2202(1)	0	1	0.011(1)
Ge(5)	8*i*	0.4411(1)	0.2897(1)	0	1	0.012(1)
Ge(6)	8*i*	0.7297(1)	0.1044(1)	0	1	0.016(1)
Ge(7)	8*i*	0.3540(1)	0.2053(1)	0	1	0.014(1)
Ge(8)	8*j*	0.6066(1)	0.3934(1)	0.6167(2)	1	0.013(1)
Ge(9)	8*j*	0.4564(1)	0.4564(1)	0.1887(2)	0.776(6)	0.013(1)
Ge(10)	16*k*	0.5076(1)	0.2651(1)	0.8100(1)	1	0.014(1)
Ge(11)	16*k*	0.6258(1)	0.2332(1)	0.8091(1)	1	0.012(1)
Ge(12)	16*k*	0.5955(1)	0.9744(1)	0.8833(1)	1	0.015(1)
E(13)[a]	8*i*	0.8457(1)	0.0684(1)	0	0.909/0.011 (7)	0.019(1)
E(14)	16*k*	0.6823(1)	0.0503(1)	0.8164(2)	0.411/0.589 (5)	0.011(1)
E(15)	16*k*	0.3679(1)	0.1349(1)	0.1848(2)	0.486/0.514 (4)	0.010(1)
E(16)	16*k*	0.4933(6)	0.4412(6)	0.1468(11)	0.09/0.02(2)	0.013(1)

[a]E(13) = Ge(13)/P(13); E(14) = Ge(14)/P(14); E(15) = Ge(15)/P(15); E(16) = Ge(16)/P(16).

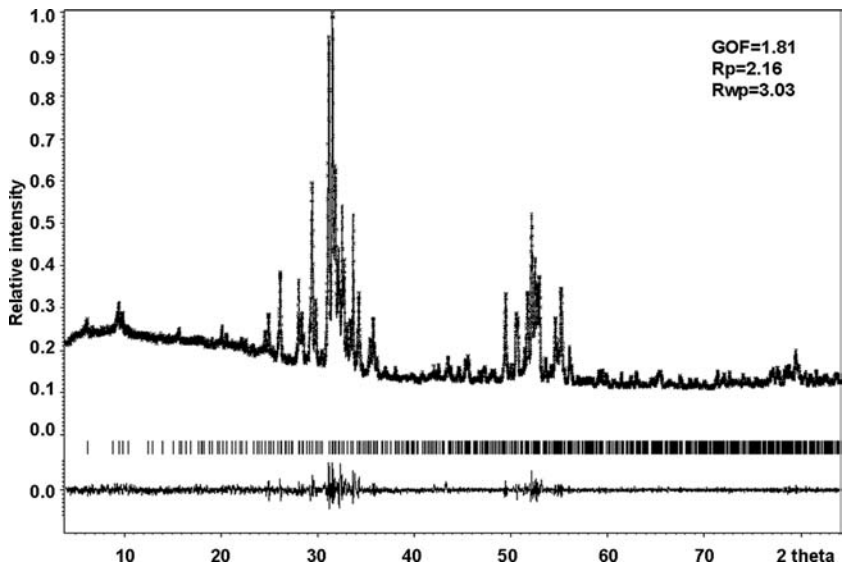

Figure 1. Experimental, calculated, and difference profiles of $Ge_{129.3}P_{42.7}Te_{21.53}$ after the Rietveld refinement. Parameters of the refinement are given in the top right corner.

compositional borders were not further investigated in this work, basically because of the low accuracy of the EDX determination of the composition of the clathrate-III phase in three-phase samples.

Our attempts to prepare a single-phase sample of $Ge_{129.3}P_{42.7}Te_{21.53}$ from elementary substances were unsuccessful. In all these cases an admixture of clathrate-I $Ge_{46-x}P_xTe_y$[23] or exclusively a mixture of $Ge_{46-x}P_xTe_y$, Ge, and GeTe was formed. According to the TG and DSC data, $Ge_{129.3}P_{42.7}Te_{21.53}$ decomposes in two steps in an Ar flow. The decomposition starts at ~875 K and proceeds with losing up to ~2 wt % of the sample weight. The second step begins at 925 K, where the material loses up to ~8 wt % of its mass. Evidently, the sum loss of 10 wt % corresponds to the total amount of phosphorus in the sample. The complicated character of the thermal decomposition of $Ge_{129.3}P_{42.7}Te_{21.53}$ might be the reason for the difficulties in preparation of this phase from pure elements. Probably, the first stage of decomposition with a loss of up to 2 wt % corresponds to the formation of the clathrate-I $Ge_{46-x}P_xTe_y$, which is more stable in a wide range of pressure and temperature.[23] Interestingly, two types of the clathrate phase (clathrate-I and clathrate-III) exist in both Ge−P−Te and Si−P−Te systems. However, in the case of silicon clathrates the difference in the synthetic conditions is no so strict, and clathrate-III can be easily prepared from elementary substances with no control of the pressure. It is not yet clear

dx.doi.org/10.1021/ic401203r | Inorg. Chem. 2013, 52, 8272−8279

whether such a difference can be associated with the difference in a distortion motif of the clathrate-I crystal structure. The silicon clathrate-I crystallizes in a primitive cubic cell, space group $Pm\bar{3}$ in contrast to a face-centered superstructure with an 8-fold increase in the unit cell volume found for the germanium clathrate-I.[23,24]

The unit cell and space symmetry of $Ge_{129.3}P_{42.7}Te_{21.53}$ derived from the XRPD data were confirmed by selected area electron diffraction (SAED) taken along several crystallographic directions. The reflection condition $0kl$, $k + l = 2n$ indicating the presence of the *n*-glide plane is clearly visible in the [100] SAED pattern (Figure 2). Absence of the $00l$, $l \neq 2n$ reflections

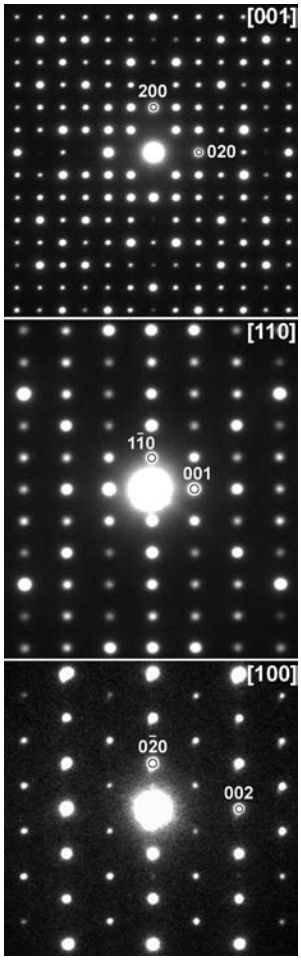

Figure 2. SAED patterns of $Ge_{129.3}P_{42.7}Te_{21.53}$ along the different zone axes [001], [110], and [100].

is also confirmed by the [100] SAED pattern. Although these reflections, forbidden by the 4_2 axis, are visible on the [110] SAED pattern, their appearance must be caused by multiple diffraction.

2. Solution and Refinement of the Crystal Structure. The crystal structure of the title compound was solved by direct methods (SHELXS-97[21]) in the tetragonal space group $P4_2/mnm$ with the unit cell parameters a = 19.948(3) and c = 10.440(2) Å. Based on the analysis of the interatomic distances, the atomic positions obtained in the direct methods solutions can be clearly separated into those forming a framework with strong covalent bonds and those located in the cavities of this framework, that is, the guest positions. Expecting that the guest positions are taken by the Te atoms only, four sites (4*g*, 8*j*, and two 8*i*) were assigned to tellurium atoms. Three of these sites appear to be fully occupied, whereas one of the 8*i* positions demonstrates only 19% occupancy by the Te atoms. The 17 sites belonging to the framework were assumed to be occupied by Ge and/or P. The subsequent refinement of the isotropic atomic displacement parameters (ADPs) and analysis of interatomic distances indicated that only 12 out of 17 sites are fully occupied by germanium. Because of the enormously high ADPs the remaining 5 sites were set as being jointly populated by germanium and phosphorus. After a detailed analysis of the interatomic distances two sites (8*j* and 16*k*) were assigned to phosphorus atoms. The distribution of the Ge and P atoms among those positions was realized in a series of subsequent refinements of the occupancy factors. The difference Fourier map around the Ge9 position revealed a high maximum of the residual electron density, located only ~0.9 Å apart. This indicates that this position is split into two: the special position 8*j*, which is occupied by Ge and the general position 16*k*, jointly occupied by Ge and P. The occupancy factors of these positions were restricted by a linear constraint to exclude their simultaneous presence in the crystal structure. The $Ge_{129.3(3)}P_{42.7(3)}Te_{21.53(3)}$ composition was deduced from the refined occupancies, which is in good agreement with the EDX data. Finally, the structure model was refined with an anisotropic approximation for ADPs for all atoms. The detailed crystallographic information is presented in Tables 1−3.

Table 3. Selected Interatomic Distances for $Ge_{129.3}P_{42.7}Te_{21.53}$

atoms	*d*, Å	atoms	*d*, Å
P(1)−Ge(8)	2.332(4)	Ge(5)−Ge(10)	2.4365(15)
P(1)−Ge(11)	2.394(2)	Ge(6)−E(14)	2.394(2)
P(1)−Ge(1)	2.399(4)	Ge(6)−E(13)	2.422(3)
P(2)−E(16)[a]	2.308(12)	Ge(7)−E(15)	2.4025(19)
P(2)−Ge(8)	2.338(3)	Ge(8)−Ge(8)	2.436(3)
P(2)−Ge(9)	2.383(3)	Ge(9)−E(16)	2.318(11)
P(2)−E(13)	2.385(3)	Ge(9)−Ge(9)	2.462(4)
P(2)−Ge(10)	2.406(3)	Ge(10)−E(14)	2.408(2)
Ge(1)−Ge(7)	2.433(2)	Ge(10)−Ge(11)	2.4416(16)
Ge(2)−Ge(12)	2.4135(12)	Ge(11)−E(15)	2.4063(19)
Ge(3)−Ge(5)	2.411(2)	Ge(12)−E(14)	2.405(2)
Ge(3)−P(16)	2.442(11)	Ge(12)−E(15)	2.4055(19)
Ge(3)−Ge(9)	2.444(3)	Ge(12)−Ge(12)	2.438(2)
Ge(4)−Ge(6)	2.418(2)	E(13)−E(13)	2.423(4)
Ge(4)−Ge(11)	2.4279(15)	E(14)−E(15)	2.333(2)
Ge(5)−Ge(7)	2.421(2)	E(16)−E(16)	2.36(2)

[a]E(13) = Ge(13)/P(13); E(14) = Ge(14)/P(14); E(15) = Ge(15)/P(15), E(16) = Ge(16)/P(16).

The refined crystal structure was further confirmed by high resolution HAADF-STEM imaging along the [001] direction (Figure 3). On HAADF-STEM images, projected atomic columns appear as dots of different brightness, roughly proportional to Z^n (n = 1−2, Z is the average atomic number along the column). No evidence of planar defects in the crystal structure has been found. The theoretical image calculated using the determined crystal structure of $Ge_{129.3}P_{42.7}Te_{21.53}$ for a thickness of 12 nm is in excellent agreement with the experimental one, confirming the correctness of the crystal structure solution. A straightforward assignment of the atomic positions on the HAADF-STEM image is difficult because of the complexity of the crystal structure. However, the most

dx.doi.org/10.1021/ic401203r | Inorg. Chem. 2013, 52, 8272−8279

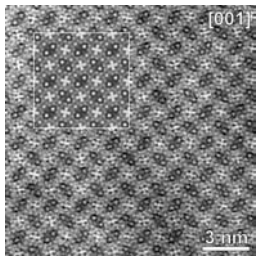

Figure 3. [001] HAADF-STEM image of $Ge_{129.3}P_{42.7}Te_{21.53}$ with the simulated image (t = 12 nm, shown as inset). The red frame indicates the borders of the unit cell.

pronounced structure details are evident. Bright dots in the centers of the black circles correspond to the guest tellurium atoms in the largest $[5^{12}6^3]$ cavities (see the structure description below). White crosses correspond to germanium atoms in the framework, matching with the columns of tellurium atoms in the smallest $[5^{12}]$ cavities. A projection of the unit cell superimposed on the experimental HAADF-STEM image is presented in Supporting Information, Figure S1.

3. Description of the Crystal Structure. The crystal structure of $Ge_{129.3}P_{42.7}Te_{21.53}$ presents a covalent framework of germanium and phosphorus atoms, which forms three types of polyhedral voids: the pentagonal dodecahedra $[5^{12}]$, larger tetrakaidecahedra $[5^{12}6^2]$, and the largest pentakaidecahedra $[5^{12}6^3]$, occurring in the ratio of 10:16:4. The symbol in the square brackets means the number and shape of the faces. For example, the symbol $[5^{12}6^2]$ corresponds to the polyhedron with 12 pentagonal and 2 hexagonal faces. A polyhedral view of the crystal structure is given in Figure 4. Tellurium atoms are

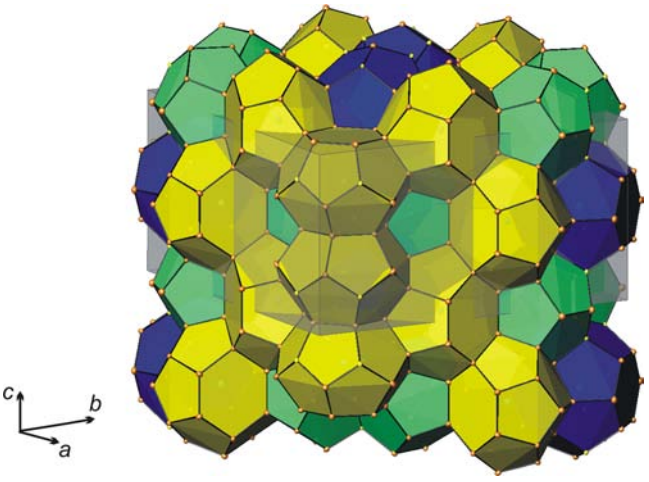

Figure 4. Polyhedral presentation of the crystal structure of $Ge_{129.3}P_{42.7}Te_{21.53}$. The shadowed parallelepiped shows the borders of the unit cell.

located at the centers of those cavities and do not form covalent bonds with the host framework. The shape of the guest cavities and the manner of their spatial packing conform to the structure type of clathrate-III. The ideal clathrate-III has a composition $[E_{172}]G^{I}{}_{10}G^{II}{}_{16}G^{III}{}_{4}$, where E denotes the framework atom, whereas G denotes the guest atom. The spatial arrangement of the cavities is illustrated in Figure 5.

The framework of $Ge_{129.3}P_{42.7}Te_{21.53}$ is vacancy free and composed of four-coordinated Ge and P atoms, occupying 18 crystallographic sites in total. Germanium occupies 12 sites, phosphorus occupies 2 sites, and 4 sites are populated mixedly by Ge and P atoms.

Tellurium atoms are located at the center of the cavities. The $[5^{12}6^2]$ and $[5^{12}6^3]$ polyhedra are fully occupied, while the occupancy of smallest $[5^{12}]$ polyhedra is only 19%. Moreover, the 2-fold position at the center of the smallest $[5^{12}]$ polyhedra is always vacant (Figure 6). Thus, the composition can be written as $[Ge_{129.3}P_{42.7}]Te^{I}{}_{1.53}\square_{8.47}Te^{II}{}_{16}Te^{III}{}_{4}$, where $\square$ denotes a vacancy at the guest position.

The crystal structure of $Ge_{129.3}P_{42.7}Te_{21.53}$ is similar to that of the silicon analogue $Si_{130}P_{42}Te_{21}$,[7] showing almost the same distribution of phosphorus atoms within the framework and partial occupancy of the small cages by Te atoms. The tendency of tellurium atoms to avoid small cavities is common for germanium- and silicon-based cationic clathrates and is also observed in the clathrates-I $Ge_{46-x}P_xTe_y$[23] and $Si_{46-x}P_xTe_y$.[24] An explanation for this might be proposed[25] by choosing the van der Waal's radius of Ge (~ 2.11 Å)[26] to estimate the effective space available for the Te atoms in the cavities. The largest distances in the smaller $[5^{12}]$ cage are 3.46 Å. Upon subtraction, the effective radius is approximately equal to 1.33 Å, that is, smaller than the covalent radius of Te (~1.39 Å).[27] Other distances in the $[5^{12}]$ cage are even shorter. In the $[5^{12}6^3]$ cage the interatomic distances vary from 3.63 to 4.09 Å. (Supporting Information, Table S1). The appearance of a relatively short distance with Ge/P(16) atoms (2.73 Å) has no visible influence on the occupancy of the large cages by Te(1) atoms. Probably, that is due to the small value of the site occupancy factor for the E(16) position. The same tendency was also noticed for the bromine hydrate $[H_2O]_{172}(Br_2)_{20}\square_{10}$[2,6] and some anionic clathrates like $K_{7.62}Si_{46}$ and $Rb_{6.15}Si_{46}$.[28] Although the employment of the combined van der Waals-ionic scheme gives a reasonable explanation of the partial occupancy of the small cages, an accurate evaluation of the size factor is more complicated. In ^{23}Na NMR experiments on Na_xSi_{136} and Na_8Si_{46} clathrates, large paramagnetic shifts were observed for the sodium nuclei inside the cages.[29] This observation excludes a description of the guest species as simple ions. For effective size considerations they are likely better described as an intermediate between "metallic" and "atomic" species.

The anionic clathrate of type-III $A_{30}[Na_xSn_{164.62-0.8x}]$ (x = 2.48; 2.88; 2.8; A = Cs, Cs/Rb)[8] was also reported in the literature. Its framework is built up of tin atoms with a small addition of sodium atoms. The framework contains vacancies, whereas all guest cavities are occupied by Cs and Rb atoms. Sodium atoms stabilize the crystal structure by filling up the space in place of the missing Sn−Sn pairs. On the contrary, the frameworks of the cationic clathrates-III $Ge_{129.3}P_{42.7}Te_{21.53}$ and $Si_{130}P_{42}Te_{21}$ are vacancy free, but Si or Ge atoms are partially substituted by phosphorus atoms to keep the charge balance. According to the Zintl formalism,[30] four-coordinated atoms of the group 14 elements are neutral, while four-coordinated phosphorus atoms have a formal charge of +1. Isolated tellurium atoms are negatively charged and can be written as Te^{2-}. According to the formula $(Ge^0)_{172-x}(P^{1+})_x(Te^{2-})_y$, the phosphorus content should be twice the tellurium content to fulfill the Zintl rule. The composition $Ge_{129.3}P_{42.7}Te_{21.53}$ is in good agreement with this formula.

4. Thermoelectric Properties. The composition $Ge_{129.3}P_{42.7}Te_{21.53}$ satisfies the Zintl rule and therefore semiconducting transport properties are to be expected. The temperature dependence of the resistivity ρ for

dx.doi.org/10.1021/ic401203r | Inorg. Chem. 2013, 52, 8272−8279

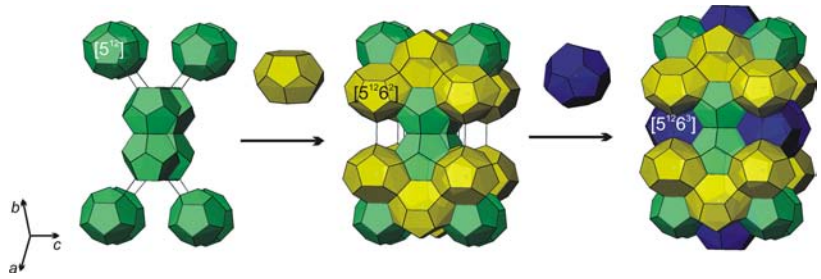

Figure 5. Spatial arrangement of the polyhedra in the crystal structure of clathrate-III.

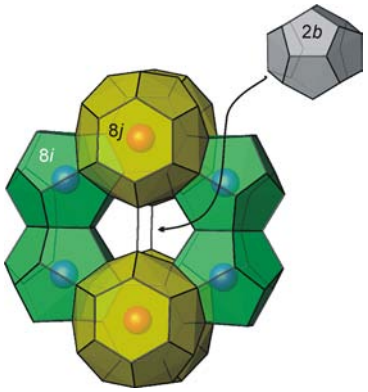

Figure 6. Location of the $[5^{12}]$ cavities, which are always empty (gray). Other $[5^{12}]$ polyhedra (green) are randomly occupied by tellurium atoms.

$Ge_{129.3}P_{42.7}Te_{21.53}$ is plotted in Figure 7a. The absolute values are relatively high compared to those of the silicon clathrate-III $Si_{132}P_{40}Te_{21.5}$,[9] with a value of $\rho \sim 10$ mΩ m at 323 K. The temperature dependence is semiconducting/insulating with ρ decreasing as the temperature increases. In the temperature range measured, the temperature dependence of the resistivity can be expressed well as simple activated by the equation

$$\rho = \rho_0 \exp(-T/\Delta) \quad \text{with} \quad \rho_0 = 96\ \text{m}\Omega\,\text{m} \quad \text{and}$$

$$\Delta = 132\ \text{K}$$

The latter value corresponds to a gap width of ~0.27 eV. This value is smaller than the band gap for cationic clathrates-I with a Ge/P framework, such as $Ge_{30}P_{16}Te_8$ (0.62 eV),[31] $Ge_{38}P_8I_8$ (0.34 eV), and $Ge_{30.6}P_{15.4}Se_8$ (0.41 eV).[32]

The positive Seebeck coefficient α shown in Figure 7b indicates that $Ge_{129.3}P_{42.7}Te_{21.53}$ is a *p*−type semiconductor. The Seebeck coefficient is large, with a value around 500 μV K^{-1} close to room temperature. The α value decreases with increasing temperature, which is in contrast to the behavior of the silicon clathrate-III $Si_{132}P_{40}Te_{21.5}$ and clathrate-I $Si_{32}P_{14}Te_7$,[9] but is in line with the electrical conductivity increasing with temperature.

The power factor *PF* which is given as the product of the electrical conductivity and the squared Seebeck coefficient is plotted in Figure 7c. The *PF* monotonically increases with temperature and reaches its maximum of around 10^{-4} W K^{-2} m^{-1} at the highest measured temperature of 660 K. The upturn of the *PF* with temperature is not so sharp, and this is due to the relatively large reduction of the Seebeck coefficient as temperature increases.

An important desirable feature of thermoelectric materials is to have a low thermal conductivity κ, considering the

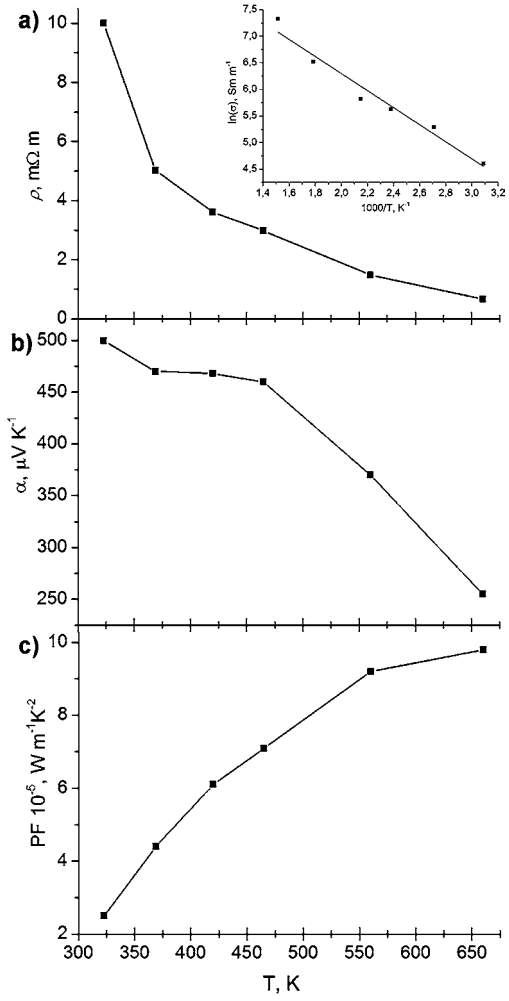

Figure 7. Temperature dependence of (a) resistivity (inset shows the linearization of the $\ln(\rho^{-1})$ versus T^{-1}); (b) Seebeck coefficient; (c) power factor for $Ge_{129.3}P_{42.7}Te_{21.53}$. Solid lines are drawn to guide the eye.

dimensionless figure of merit $ZT = PF \times T/\kappa$. As shown in Figure 8, the thermal conductivity of $Ge_{129.3}P_{42.7}Te_{21.53}$ is quite low, taking values $\kappa < 0.92$ W K^{-1} m^{-1} throughout the temperature region measured. These values are significantly lower than the $1 < \kappa < 1.5$ W K^{-1} m^{-1} (300 K < *T* < 1000 K) reported for the $Si_{132}P_{40}Te_{21.5}$ clathrate which may be in part due to the heavier germanium atoms. Taking into account the comparatively low electrical conductivity, the electronic part of the thermal conductivity was estimated using the Wiedemenn−Franz law[33] to constitute less than 10% of the total thermal conductivity. Consequently, the thermal conductivity is mainly phononic, and its low value can be explained by two principal

dx.doi.org/10.1021/ic401203r | Inorg. Chem. 2013, 52, 8272−8279

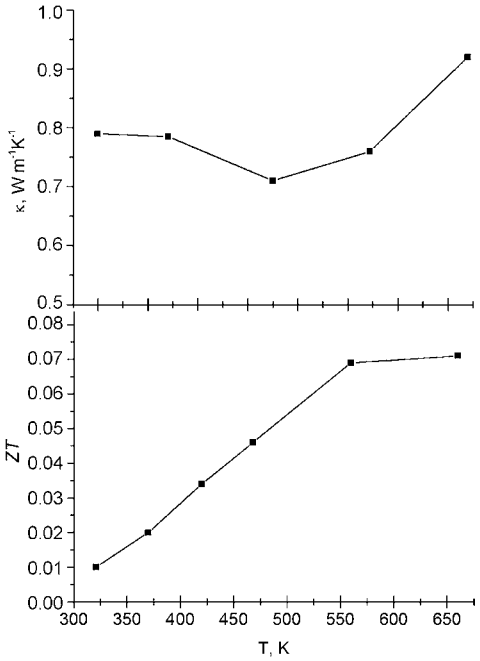

Figure 8. Temperature dependence of thermal conductivity (top) and ZT (bottom) for $Ge_{129.3}P_{42.7}Te_{21.53}$. Solid lines are drawn to guide the eye.

factors: the large unit cell volume and the rattling modes of the guest atoms inside the cages. They both ensure effective scattering of the heat-carrying phonons.

The estimated *ZT* of $Ge_{129.3}P_{42.7}Te_{21.53}$ is plotted in Figure 8. Since the temperature range of the measurements of ρ, α, and κ do not overlap perfectly, the thermal conductivity values were estimated from the measured data. *ZT* increases with increasing temperature and appears to saturate above 550 K. This is due to the saturation tendency of the power factor and the slight upturn in thermal conductivity at the highest temperatures. *ZT* reaches a maximum value of slightly more than 0.07 at the highest temperature of 660 K. As a first report on a nonoptimized compound, this value is promising. The power factor can be expected to increase with optimum doping of the carrier concentration. $Ge_{129.3}P_{42.7}Te_{21.53}$ shows a significantly lower thermal conductivity than its silicon counterpart; further work to modify its thermoelectric properties should prove to be of interest.

CONCLUSIONS

A new cationic clathrate $Ge_{129.3}P_{42.7}Te_{21.53}$ belonging to the rare clathrate-III structure type was synthesized from GeP, Ge, and Te as a single phase. The cationic framework composed from germanium and phosphorus atoms exhibits three types of polyhedral cages, sharing their faces and trapping guest tellurium atoms. The occupancy of the smallest cages is only 19% and leads to vacancies in the guest positions. Varying experimental conditions allowed us to synthesize phases with different Ge/P ratio, presenting a homogeneity range with general composition $Ge_{172-x}P_xTe_y$.

The $Ge_{129.3}P_{42.7}Te_{21.53}$ composition and measured transport properties are in agreement with the Zintl concept. The temperature dependence of the electrical resistivity is semiconducting/insulating. The high positive Seebeck coefficient reflects that $Ge_{129.3}P_{42.7}Te_{21.53}$ is a *p*-type semiconductor, which is typical for clathrates with a positively charged framework. Combined with a quite low thermal conductivity, $\kappa < 0.92$ W K^{-1} m^{-1}, this leads to a moderate thermoelectric figure of merit *ZT* with a maximum of 0.07 at 660 K.

ASSOCIATED CONTENT

Supporting Information

X-ray crystallographic data for $Ge_{129.3}P_{42.7}Te_{21.53}$ in CIF format, fragment of the structure superimposed on HAADF-STEM image, interatomic distances for Te atoms. This material is available free of charge via the Internet at http://pubs.acs.org.

AUTHOR INFORMATION

Corresponding Author

*E-mail: shev@inorg.chem.msu.ru. Phone: (+7-495) 939 20 74. Fax: (+7-495) 939 09 98.

Notes

The authors declare no competing financial interest.

ACKNOWLEDGMENTS

M.A.K. thanks EMAT, University of Antwerp, for supporting her stay at EMAT and Mr. D. Batuk and Mrs. M. Batuk for help with EM investigations. T.M. and A.V.S. thank the Open Research Institute Program of NIMS and the bilateral MSU-NIMS research initiative. This work is supported in part by the Lomonosov Moscow State University program of development and by the Russian Foundation for Basic Research (Grant # 13-03-00571).

REFERENCES

(1) Davy, H. *Philos. Trans. R. Soc. London* **1811**, *101*, 155.
(2) Jeffrey, G. A. In *Inclusion Compounds*; Atwood, J. L., Davies, J. E. D., MacNichol, D., Eds.; Academic Press Inc.: London, U.K., 1984.
(3) Kasper, J. S.; Hagenmuller, P.; Pouchard, M.; Cros, C. *Science* **1965**, *150*, 1713−1714.
(4) (a) Nolas, G. S.; Cohn, J. L.; Slack, G. A.; Schujman, S. B. *Appl. Phys. Lett.* **1998**, *73*, 178−180. (b) Saramat, A.; Svensson, G.; Palmqvist, A. E. C.; Stiewe, C.; Mueller, E.; Platzek, D.; Williams, S. G. K.; Rowe, D. M.; Bryan, J. D.; Stucky, G. D. *J. Appl. Phys.* **2006**, *99* (023708), 1−5. (c) Zhang, H.; Borrmann, H.; Oeschler, N.; Candolfi, C.; Schnelle, W.; Schmidt, M.; Burkhardt, U.; Baitinger, M.; Zhao, J. T.; Grin, Yu. *Inorg. Chem.* **2011**, *50*, 1250−1257.
(5) (a) Kovnir, K. A.; Shevelkov, A. V. *Russ. Chem. Rev.* **2004**, *73*, 923−938. (b) Shevelkov, A. V.; Kovnir, K. A. *Struct. Bonding (Berlin)* **2011**, *139*, 97−144.
(6) Udachin, K. A.; Enright, G. D.; Ratcliffe, C. I.; Ripmeester, J. A. *J. Am. Chem. Soc.* **1997**, *119*, 11481−11486.
(7) Zaikina, J. V.; Kovnir, K. A.; Haarmann, F.; Schnelle, W.; Burkhardt, W. U.; Borrmann, H.; Schwarz, U.; Grin, Yu.; Shevelkov, A. V. *Chem.—Eur. J.* **2008**, *14*, 5414−5422.
(8) Bobev, S.; Sevov, S. C. *J. Am. Chem. Soc.* **2001**, *123*, 3389−3390.
(9) Zaikina, J. V.; Mori, T.; Kovnir, K.; Teschner, D.; Senyshyn, A.; Schwarz, U.; Grin, Yu.; Shevelkov, A. V. *Chem.—Eur. J.* **2010**, *16*, 12582−12589.
(10) Shevelkov, A. V.; Shatruk, M. M. *Russ. Chem. Bull.* **2001**, *50*, 337−352.
(11) (a) Menke, H.; von Schnering, H. G. *Naturwissenschaften* **1972**, *59*, 420−420. (b) Menke, H.; von Schnering, H. G. *Z. Anorg. Allg. Chem.* **1973**, *395*, 223−238.
(12) Kirsanova, M. A.; Olenev, A. V.; Abakumov, A. M.; Bykov, M. A.; Shevelkov, A. V. *Angew. Chem., Int. Ed.* **2011**, *50*, 2371−2374.
(13) Nolas, G. S.; Morelli, D. T.; Tritt, T. M. *Annu. Rev. Mater. Sci.* **1999**, *29*, 89−116.
(14) Uher, C. *Thermoelectrics Handbook Macro to Nano*; Rowe, D. M., Ed.; CRC Press, Boca Raton. FL, 2006.
(15) Rowe, D. M. *J. Power Sources* **1987**, *19*, 247−259.
(16) Wood, C.; Emin, D. *Phys. Rev. B* **1984**, *29*, 4582−4587.

(17) (a) Mori, T.; Berthebaud, D.; Nishimura, T.; Nomura, A.; Shishido, T.; Nakajima, K. *Dalton Trans.* **2010**, *39*, 1027−1030. (b) Maruyama, S.; Miyazaki, Y.; Hayashi, K.; Kajitani, T.; Mori, T. *Appl. Phys. Lett.* **2012**, *101* (152101), 1−4.
(18) Terasaki, I.; Sasago, Y.; Uchinokura, K. *Phys. Rev. B* **1997**, *56*, R12685−R12687.
(19) Brown, S. R.; Kauzlarich, S. M.; Gascoin, F.; Snyder, G. J. *Chem. Mater.* **2006**, *18*, 1873−1877.
(20) Brauer, G. *Handbuch der Präparativen Anorganischen Chemie*; F. Enke Verlag: Stuttgart, Germany, 1975.
(21) Sheldrick, G. M. *Acta Crystallogr., Sect. A* **2008**, *64*, 112−122.
(22) Koch, C. Ph.D. Thesis, Arizona State University, Phoenix, AZ, 2002.
(23) Kirsanova, M. A.; Reshetova, L. N.; Olenev, A. V.; Abakumov, A. M.; Shevelkov, A. V. *Chem.—Eur. J.* **2011**, *17*, 5719−5726.
(24) Zaikina, J. V.; Kovnir, K. A.; Burkhardt, U.; Schnelle, W.; Haarmann, F.; Schwarz, U.; Grin, Yu.; Shevelkov, A. V. *Inorg. Chem.* **2009**, *48*, 3720−3730.
(25) Cros, C.; Pouchard, M.; Hagenmuller, P. *J. Solid State Chem.* **1970**, *2*, 570−581.
(26) Mantina, M.; Chamberlin, A. C.; Valero, R.; Cramer, C. J.; Truhlar, D. G. *J. Phys. Chem. A* **2009**, *113*, 5806−5812.
(27) Alcock, N. W. *Inorganic Chemistry*; Ellis Horwood: New York, 1990.
(28) Ramachandran, G. K.; McMillan, P. F. *J. Solid State Chem.* **2000**, *154*, 626−634.
(29) (a) Gryko, J.; McMillan, P. F.; Sankey, O. F. *Phys. Rev. B* **1996**, *54*, 3037−3039. (b) Gryko, J.; McMillan, P. F.; Marzke, R. F.; Dodokin, A. P.; Demkov, A. A.; Sankey, O. F. *Phys. Rev. B* **1998**, *57*, 4172−4179. (c) Shimizu, F.; Maniwa, Y.; Kume, K.; Kawaji, H.; Yamanaka, S.; Ishikawa, M. *Phys. Rev. B* **1996**, *54*, 13242−13246. (d) Shimizu, F.; Maniwa, Y.; Kume, K.; Kawaji, H.; Yamanaka, S.; Ishikawa, M. *Synth. Met.* **1997**, *86*, 2141−2142.
(30) *Chemistry, structure and bonding of Zintl phases and ions*; Kauzlarich, M. S., Ed.; VCH Publishers: New York, 1996.
(31) Kishimoto, K.; Akai, K.; Muraoka, N.; Koyanagi, T.; Matsuura, M. *Appl. Phys. Lett.* **2006**, *89*, 172106 (1−3).
(32) Kirsanova, M. A.; Mori, T.; Maruyama, S.; Matveeva, M.; Batuk, D.; Abakumov, A.; Gerasimenko, A. V.; Olenev, A. V.; Grin, Y. N.; Shevelkov, A. V. *Inorg. Chem.* **2013**, *52*, 577−588.
(33) White, M. A. *Properties of Materials*; Oxford University Press: New York, 1999.